

Electronic supplementary information for

Electronic structures and ferroelectric properties of LaWN₃ ultrathin films

Wan Chen¹, Kai Gao¹, Chunju Hou², Yi Yang,^{1*}

¹ College of Rare Earths and Faculty of Materials, Metallurgy and Chemistry, Jiangxi University of Science and Technology, Ganzhou, 341000, China

² School of Science, Jiangxi University of Science and Technology, Ganzhou, 341000, China

*Corresponding author, e-mail address: yangyisouth@yeah.net

Surface stability

To assess the surface stability, the surface energies (E_{surf}) of the (110) surface of the *R3c* phase and the (001) surface of the cubic phase were calculated according to an approach proposed by Padilla and Vanderbilt.^{1,2} PBE functional was used in calculating the surface energies. For LaN-terminated surface, the E_{surf} is calculated as follows:

$$E_{\text{surf}}^{\text{LaN}} = \frac{1}{2S} (E_{\text{slab}}^{\text{LaN}} - N_{\text{bulk}} E_{\text{bulk}} + E_{\text{WN}_2} + \Delta\mu_{\text{WN}_2}) \quad (1)$$

where $E_{\text{slab}}^{\text{LaN}}$ (eV), E_{bulk} and E_{WN_2} are the total energies of LaN-terminated slab, the LaWN₃ bulk and the binary WN₂, respectively. S is the area of the surface. N_{bulk} is the number of formula units of LaWN₃ in the slab. $\Delta\mu_{\text{WN}_2}$ is the relative chemical potential of binary WN₂ with respect to the total energy of WN₂. Similarly, For WN₂-terminated surface, the E_{surf} is calculated according to the following equation:

$$E_{\text{surf}}^{\text{WN}_2} = \frac{1}{2S} (E_{\text{slab}}^{\text{WN}_2} - N_{\text{bulk}} E_{\text{bulk}} - E_{\text{WN}_2} - \Delta\mu_{\text{WN}_2}) \quad (2)$$

To ensure the stability of the LaWN₃ bulk and avoid the formation of the binaries WN₂ and LaN, the chemical potential must satisfy the following condition:

$$E_f < \Delta\mu_{\text{WN}_2} < 0$$

where E_f is the formation energy of the LaWN₃ bulk relative to the stable binaries WN₂ and LaN. Calculated E_f values are -1.54 eV and -1.29 eV for the *R3c* and cubic phases, respectively. The surface energies can also be calculated by utilizing the chemical potential of $\Delta\mu_{\text{LaN}}$ as a variable. Two descriptions based on $\Delta\mu_{\text{WN}_2}$ and $\Delta\mu_{\text{LaN}}$ are equivalent since there is a relationship: $\Delta\mu_{\text{WN}_2} + \Delta\mu_{\text{LaN}} = E_f$. By substituting this equation into equation (1) and (2), the surface energies can be calculated as a function of $\Delta\mu_{\text{LaN}}$. Symmetric slabs with the thickness of 8 UC are utilized to simulate the surfaces of the bulks.

We examine which termination exhibits higher stability when the LaWN₃ ultrathin films are relatively thick, e.g., in the 8-UC case. Fig. S1a shows the surface energies for two types of terminations as a function of the chemical potential of binary WN₂ ($\Delta\mu_{\text{WN}_2}$) for the *R3c* phase. The allowed range of $\Delta\mu_{\text{WN}_2}$ is from -1.54 eV to 0 eV, which corresponds to LaN-rich (or WN₂-poor) and WN₂-rich conditions, respectively. We find that LaN-termination is more stable than the WN₂-case at most range of $\Delta\mu_{\text{WN}_2}$, except that the WN₂-surface has a slightly lower surface energy at the WN₂-rich condition. For a comparison, Fig. S1b shows the surface energies of (001)_c surfaces for the cubic phase.

A similar rule of termination-dependent stability occurs to the cubic phase, suggesting that LaN-surface is more favorable to appear in the LaWN₃ films at thermodynamic equilibrium. It is worth noting that SrO-termination also show higher stability than TiO₂-termination for the (001) surface of oxide perovskite SrTiO₃.^{3, 4} This finding implies some similarity of surface stability between nitride and oxide perovskites.

We calculate the average surface energy for two types of surfaces to be 1.38 J/m², which is independent of $\Delta\mu_{\text{WN}_2}$. LaWN₃ has a surface energy close to those of oxide perovskites. The surface energies of the (001) surfaces of typical perovskites (e.g., CaTiO₃, SrTiO₃ and BaTiO₃) were calculated to be around 1.1~1.3 J/m².⁵ This result implies that LaWN₃ has a similar inter-layer interaction strength as oxide perovskites and indicates that 2D LaWN₃ may be fabricated since many 2D oxide perovskites have been synthesized.⁶⁻⁸ Notably, the surface energies of both nitride and oxide perovskites are one order of magnitude larger than the values of halide perovskites.⁹

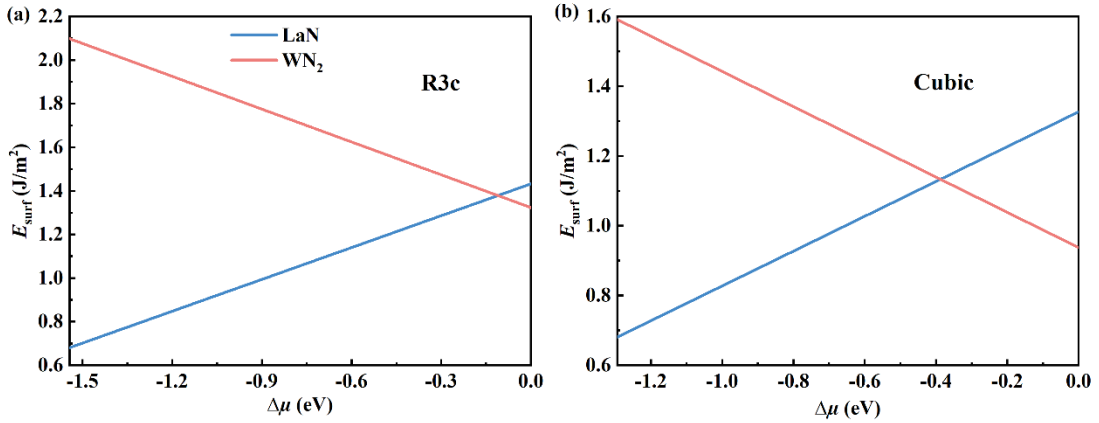


Fig. S1 Surface energies of the LaN- and WN₂-terminated surfaces as a function of chemical potential of WN₂: (a) R3c phase, (b) Cubic phase. The allowed range of $\Delta\mu_{\text{WN}_2}$ is from -1.54 eV to 0 eV in the R3c phase, which corresponds to LaN-rich (or WN₂-poor) and WN₂-rich conditions, respectively. The allowed range of $\Delta\mu_{\text{WN}_2}$ is from -1.29 eV to 0 eV in the cubic phase. The average surface energy for these two types of terminations is calculated to be 1.13 J/m² for the cubic phase, which is slightly lower than that of R3c phase (1.38 J/m²).

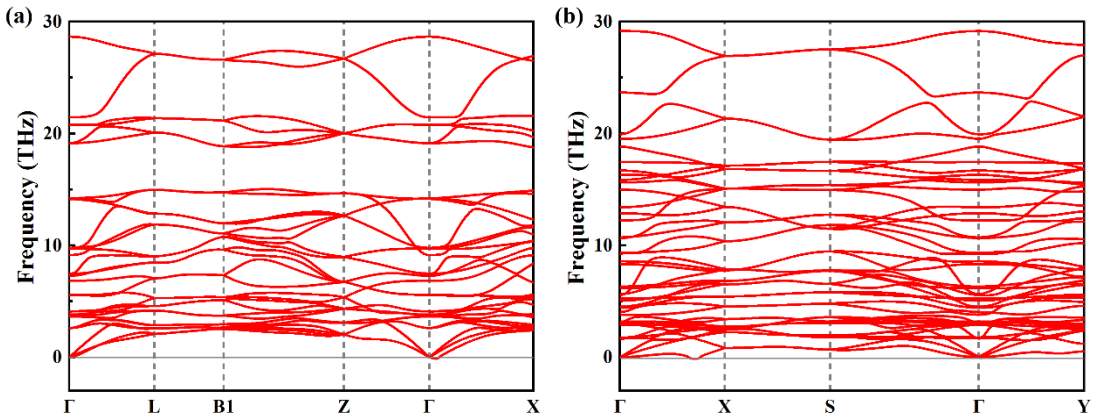


Fig. S2 Phonon dispersion curves of (a) bulk and (b) 1-UC LaN-2D ultrathin film for LaWN₃.

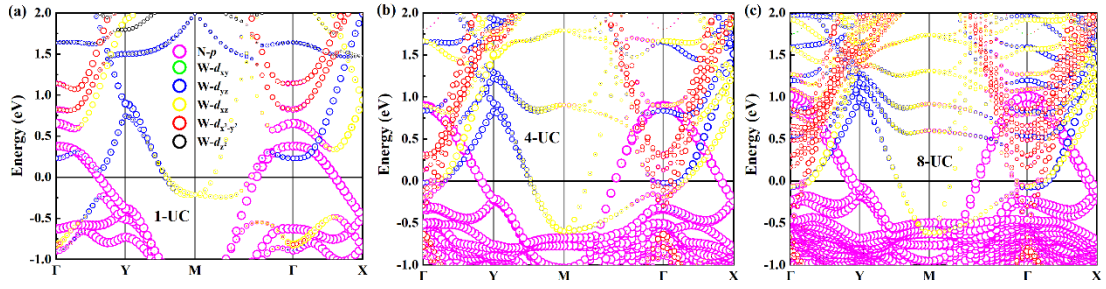


Fig. S3 Orbital-projected band structures for WN₂-2D structures: (a) 1-UC, (b) 4-UC and (c) 8-UC.

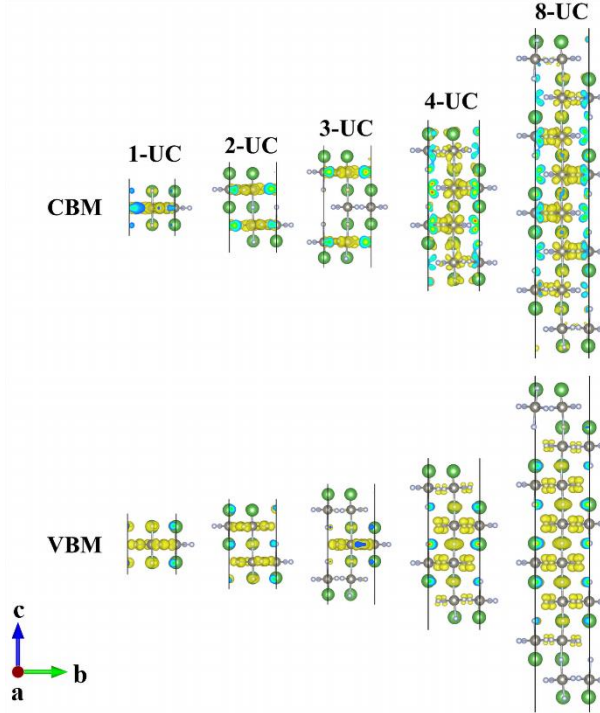


Fig. S4 Charge densities of the CBM and VBM states for LaN-2D structures with the thickness 1~8-UC. The CBM states are mainly contributed by W dx^2-y^2 orbital with an in-plane character for 1~3-UC ultrathin films. In contrast, the CBM states consist of d_{yz} orbitals with an out-of-plane character for 4~8-UC ultrathin films. The VBM states are mainly contributed by in-plane p_x and p_y orbitals of N for 1~3-UC cases. For 4~8-UC cases, the VBM states are mainly contributed by the p_y and p_z orbitals of N.

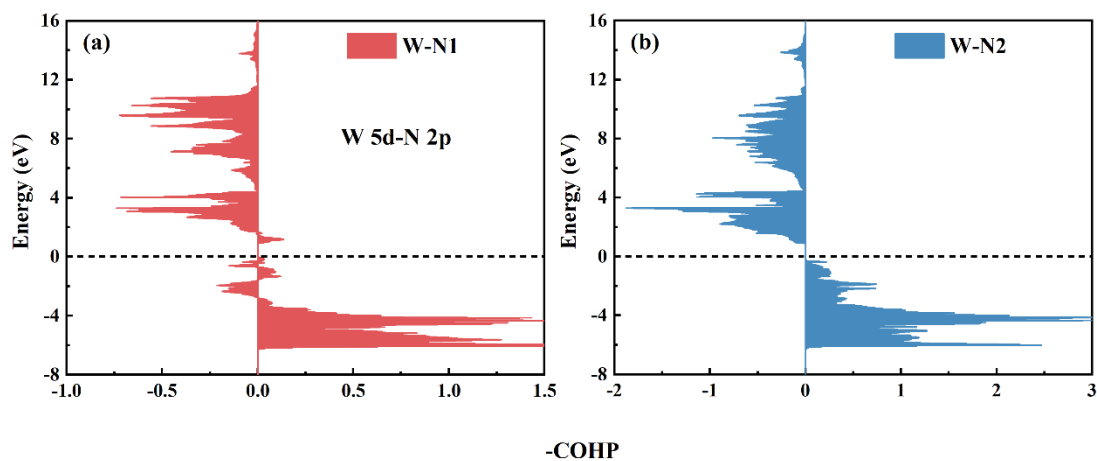


Fig. S5 The crystal orbital Hamiltonian population (COHP) of the W-N bonds in the bulk. There are two kinds of W-N bonds in the bulk structure, i.e., W-N1 bond with the length of 2.12 Å in (a) and W-N2 bond with the length of 1.90 Å in (b). $-\text{COHP}$ is plotted as convention so that negative (or positive) part stands for the antibonding (or bonding) interaction.

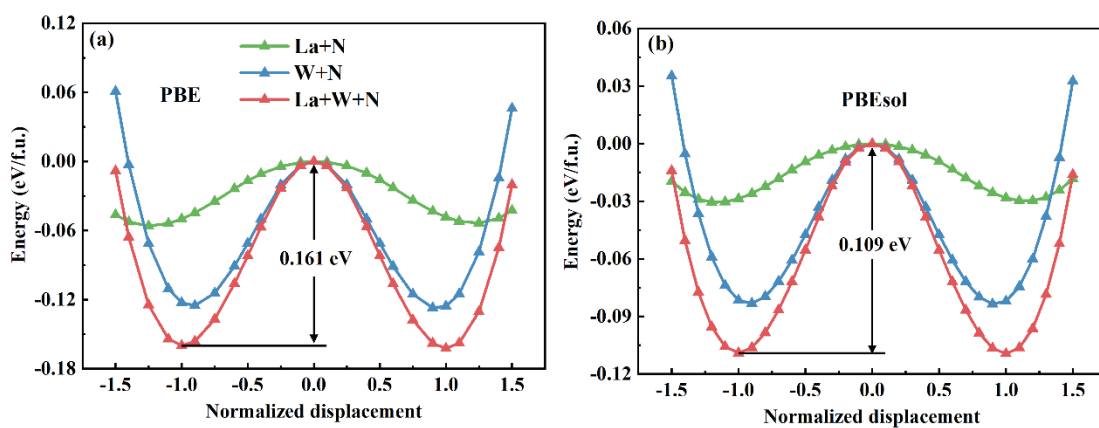


Fig. S6 Energy as a function of displacement for partial modes and full mode in LaWN_3 bulk calculated by PBE and PBEsol functionals.

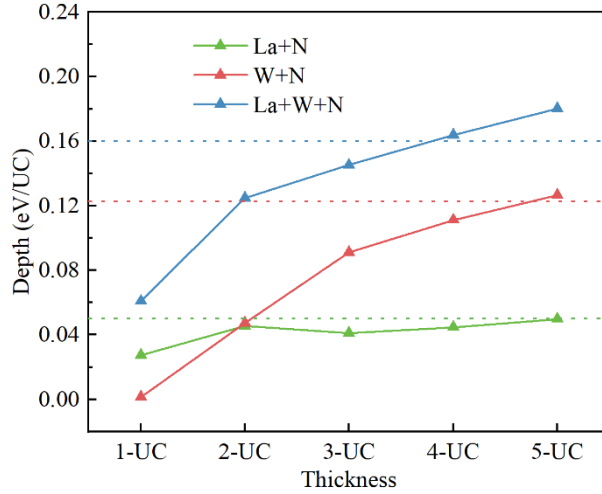


Fig. S7 Depth of double-wells obtained from PBE method for La+N and W+N partial modes as well as the full mode as a function of the thickness. The dashed lines mark the well-depths of corresponding modes in the bulk. The depth of each ultrathin film is divided by the number of UC in this film.

Table S1. Structural parameters (a and c) of $R3c$ bulk calculated by LDA, PBE and PBEsol. The experimental (Expt.) and calculated (Cal.) values from the references are also listed for a comparison. It is seen that the calculated values in this work are in good agreement with experimental and theoretical values in previous works (Ref.).

a (Å)	c (Å)	Method	Expt./Cal.	Ref
5.622	13.617	LDA	Cal.	This work
5.704	13.914	PBE	Cal.	This work
5.653	13.707	PBEsol	Cal.	This work
5.633	13.799	\	Expt.	Ref. ¹⁰
5.67	13.79	\	Expt.	Ref. ¹¹
5.713	13.960	PBE	Cal.	Ref. ¹²
5.630	13.646	LDA	Cal.	Ref. ¹³

Table S2. In-plane lattice constants (a and b) of LaN-2D and WN₂-2D as a function of the thickness. The estimated thicknesses (c) of the 2D structures are also listed.

Thickness	LaN-2D			WN ₂ -2D		
	a (Å)	b (Å)	c (Å)	a (Å)	b (Å)	c (Å)
1UC	5.373	5.352	26.248	5.495	5.511	25.250
2UC	5.500	5.458	29.289	5.499	5.522	29.270
3UC	5.539	5.502	32.923	5.505	5.509	33.408
4UC	5.556	5.525	36.728	5.506	5.514	37.463
5UC	5.566	5.537	40.621	5.511	5.517	41.491
6UC	5.575	5.548	44.488	5.515	5.522	45.496
8UC	5.583	5.556	52.366	5.524	5.529	53.506

Table S3. Calculated BEC tensors Z_{ij} for La, W, and N in the bulk LaWN₃.

	Z_{xx}	Z_{yy}	Z_{zz}	Z_{xy}	Z_{xz}	Z_{yx}	Z_{yz}	Z_{zx}	Z_{zy}
La	4.522	4.522	4.068	0.451	0.000	-0.451	0.000	0.000	0.000
La	4.522	4.522	4.068	-0.451	0.000	0.451	0.000	0.000	0.000
W	10.598	10.598	6.982	0.830	0.000	-0.831	-0.001	0.000	0.000
W	10.600	10.598	6.982	-0.831	0.000	0.831	-0.001	0.000	0.000
N	-6.301	-3.779	-3.683	-1.211	1.713	-1.507	0.825	1.707	0.675
N	-5.587	-4.494	-3.683	-1.920	1.571	-1.623	1.072	1.438	1.141
N	-5.586	-4.494	-3.683	1.920	-1.571	1.623	1.072	-1.438	1.141
N	-6.302	-3.779	-3.683	1.210	-1.714	1.507	0.825	-1.707	0.675
N	-3.233	-6.847	-3.683	-0.264	-0.142	-0.561	-1.897	-0.269	-1.816
N	-3.233	-6.847	-3.683	0.266	0.142	0.561	-1.897	0.269	-1.816

Table S4. Calculated BEC tensors Z_{ij} of 1-UC LaWN_3 ultrathin film. The Z_{xx} of La and N ions in two surface LaN-layers are shown as bold. Z_{xx} is responsible for the ferroelectric polarization along a direction.

1UC	Z_{xx}	Z_{xy}	Z_{xz}	Z_{yx}	Z_{yy}	Z_{yz}	Z_{zx}	Z_{zy}	Z_{zz}
La1	4.391	-0.453	0.096	-0.500	4.409	0.151	0.017	0.012	0.467
La2	4.388	0.450	-0.086	0.492	4.399	0.134	-0.006	0.012	0.467
W1	10.338	0.470	0.011	-1.118	12.260	-0.004	0.014	-0.003	0.719
N1	-5.151	2.681	-0.001	2.747	-6.657	0.015	-0.007	0.004	-0.247
N2	-6.393	2.723	-0.007	2.991	-6.824	0.006	-0.009	0.004	-0.200
N3	-3.788	-0.071	0.197	0.213	-3.796	-0.011	0.001	0.002	-0.602
N4	-3.785	0.066	-0.209	-0.211	-3.788	0.007	-0.010	0.003	-0.603

Table S5. Calculated BEC tensors Z_{ij} of 2-UC LaWN_3 ultrathin film. The Z_{xx} of La and N ions in two surface LaN-layers are shown as bold (La1, La3, N5 and N7). The Z_{xx} of La and N ions in inner LaN-layers are shown as blue colour (La2 and N6).

2UC	Z_{xx}	Z_{xy}	Z_{xz}	Z_{yx}	Z_{yy}	Z_{yz}	Z_{zx}	Z_{zy}	Z_{zz}
La1	4.451	-0.359	0.434	-0.400	4.402	0.250	0.018	0.106	0.765
La2	4.192	0.001	0.015	-0.004	4.305	0.788	0.013	0.016	0.341
La3	4.456	0.356	-0.410	0.396	4.398	0.247	0.008	0.110	0.764
W1	8.826	0.270	-0.642	-0.675	10.778	0.289	0.075	0.077	0.946
W2	8.815	0.269	0.696	-0.672	10.771	-0.287	-0.017	-0.076	0.951
N1	-4.349	2.107	0.104	2.142	-6.354	0.098	-0.004	0.087	-0.362
N2	-4.346	2.107	-0.130	2.139	-6.348	-0.078	-0.024	-0.072	-0.363
N3	-5.800	2.396	-0.148	2.865	-5.794	-0.172	-0.056	0.002	-0.303
N4	-5.799	2.392	0.110	2.863	-5.794	0.191	0.016	0.015	-0.302
N5	-3.639	0.075	0.468	0.017	-3.535	0.101	-0.005	0.042	-0.788
N6	-3.172	0.000	-0.007	0.003	-3.300	-0.422	-0.008	-0.006	-0.857
N7	-3.635	-0.078	-0.490	-0.017	-3.531	0.104	-0.016	0.042	-0.791

Table S6. Calculated BEC tensors Z_{ij} of 3-UC LaWN₃ ultrathin film. The Z_{xx} of La and N ions in two surface LaN-layers are shown as bold. The Z_{xx} of La and N ions in inner LaN-layers are shown as blue colour.

3UC	Z_{xx}	Z_{xy}	Z_{xz}	Z_{yx}	Z_{yy}	Z_{yz}	Z_{zx}	Z_{zy}	Z_{zz}
La1	4.450	-0.328	0.512	-0.309	4.365	0.192	-0.318	0.520	1.768
La2	4.197	-0.064	0.201	-0.058	4.335	0.815	0.005	0.001	0.228
La3	4.200	0.056	-0.164	0.059	4.331	0.817	0.043	-0.034	0.220
La4	4.460	0.326	-0.476	0.322	4.365	0.218	0.317	0.517	1.752
W1	8.262	0.192	-0.742	-0.528	10.394	0.240	0.098	0.155	0.915
W2	8.793	0.397	0.038	-0.864	10.762	-0.011	0.037	0.005	1.016
W3	8.273	0.193	0.817	-0.526	10.389	-0.243	-0.032	-0.145	0.920
N1	-4.077	1.923	0.059	1.938	-6.208	0.017	0.036	0.277	-0.437
N2	-4.450	2.098	-0.020	2.227	-6.451	-0.002	-0.018	0.009	-0.453
N3	-4.088	1.929	-0.096	1.945	-6.216	-0.024	-0.065	-0.251	-0.427
N4	-5.612	2.327	-0.186	2.775	-5.718	-0.164	-0.247	-0.003	-0.453
N5	-5.466	2.342	-0.030	2.926	-5.549	0.016	-0.023	0.009	-0.430
N6	-5.624	2.326	0.126	2.775	-5.713	0.192	0.200	0.027	-0.448
N7	-3.559	0.146	0.515	0.026	-3.385	0.201	0.069	0.125	-1.116
N8	-3.101	-0.059	0.216	-0.051	-3.163	-0.356	-0.041	-0.005	-0.962
N9	-3.099	0.054	-0.233	0.055	-3.160	-0.357	0.028	-0.005	-0.963
N10	-3.558	-0.137	-0.537	-0.026	-3.379	0.184	-0.088	0.115	-1.129

Table S7. Calculated BEC tensors Z_{ij} of 4-UC LaWN_3 ultrathin film. The Z_{xx} of La and N ions in two surface LaN-layers are shown as bold. The Z_{xx} of La and N ions in inner LaN-layers are shown as blue colour.

4UC	Z_{xx}	Z_{xy}	Z_{xz}	Z_{yx}	Z_{yy}	Z_{yz}	Z_{zx}	Z_{zy}	Z_{zz}
La1	4.456	-0.311	0.547	-0.244	4.360	0.160	0.074	0.631	1.770
La2	4.207	-0.101	0.243	-0.060	4.339	0.817	0.051	-0.128	0.756
La3	4.203	-0.004	0.020	-0.003	4.359	0.845	0.026	-0.055	0.431
La4	4.208	0.094	-0.205	0.058	4.337	0.823	0.025	-0.092	0.814
La5	4.463	0.311	-0.509	0.252	4.360	0.174	-0.038	0.655	1.771
W1	8.013	0.177	-0.751	-0.438	10.284	0.277	0.087	0.115	1.013
W2	8.572	0.333	-0.133	-0.841	10.524	-0.177	0.031	0.021	1.096
W3	8.572	0.334	0.207	-0.844	10.518	0.162	0.031	-0.013	1.095
W4	8.009	0.179	0.819	-0.435	10.277	-0.281	-0.030	-0.108	1.019
N1	-3.954	1.838	0.045	1.851	-6.177	-0.038	0.274	0.601	-0.986
N2	-4.321	2.007	-0.015	2.135	-6.368	-0.041	-0.044	0.022	-0.466
N3	-4.320	2.006	-0.024	2.133	-6.365	0.040	-0.006	-0.022	-0.454
N4	-3.956	1.840	-0.080	1.853	-6.179	0.041	-0.322	-0.584	-0.967
N5	-5.527	2.294	-0.217	2.732	-5.693	-0.143	-0.486	0.008	-0.720
N6	-5.409	2.346	-0.053	2.892	-5.504	0.011	-0.052	0.016	-0.460
N7	-5.414	2.348	-0.005	2.893	-5.503	0.019	-0.004	0.022	-0.457
N8	-5.530	2.293	0.162	2.732	-5.690	0.170	0.445	0.031	-0.714
N9	-3.533	0.182	0.536	0.025	-3.335	0.268	0.364	0.293	-0.709
N10	-3.069	-0.083	0.267	-0.053	-3.088	-0.356	-0.017	0.038	-1.064
N11	-3.073	-0.004	-0.007	0.002	-3.047	-0.237	-0.015	-0.016	-0.978
N12	-3.066	0.079	-0.286	0.057	-3.082	-0.359	-0.006	0.033	-1.064
N13	-3.527	-0.178	-0.558	-0.026	-3.330	0.260	-0.388	0.275	-0.726

Table S8. Calculated BEC tensors Z_{ij} of 5-UC LaWN₃ ultrathin film. The Z_{xx} of La and N ions in two surface LaN-layers are shown as bold. The Z_{xx} of La and N ions in inner LaN-layers are shown as blue colour.

5UC	Z_{xx}	Z_{xy}	Z_{xz}	Z_{yx}	Z_{yy}	Z_{yz}	Z_{zx}	Z_{zy}	Z_{zz}
La1	4.462	-0.303	0.563	-0.220	4.361	0.158	2.219	-1.208	-1.295
La2	4.218	-0.109	0.262	-0.051	4.351	0.815	0.482	0.477	2.779
La3	4.211	-0.036	0.052	-0.016	4.349	0.857	-0.088	-0.036	0.805
La4	4.213	0.042	-0.016	0.002	4.352	0.855	0.141	0.004	0.813
La5	4.222	0.111	-0.228	0.039	4.352	0.812	-0.495	0.467	2.870
La6	4.469	0.303	-0.531	0.217	4.360	0.159	-2.289	-1.373	-1.338
W1	7.891	0.169	-0.747	-0.399	10.225	0.285	0.004	-0.086	0.337
W2	8.448	0.314	-0.163	-0.783	10.441	-0.192	-0.081	-0.063	1.339
W3	8.482	0.300	0.030	-0.870	10.350	0.002	0.032	-0.012	1.585
W4	8.435	0.313	0.222	-0.778	10.437	0.195	0.152	0.048	1.347
W5	7.884	0.171	0.806	-0.396	10.226	-0.286	0.086	0.091	0.281
N1	-3.895	1.798	0.037	1.813	-6.163	-0.053	1.487	2.700	-1.498
N2	-4.257	1.965	-0.010	2.092	-6.355	-0.067	0.054	0.468	-0.216
N3	-4.236	1.943	-0.017	2.071	-6.293	0.018	0.009	0.007	-0.063
N4	-4.251	1.960	-0.025	2.087	-6.353	0.099	-0.071	-0.421	-0.205
N5	-3.891	1.798	-0.068	1.810	-6.163	0.075	-1.480	-2.670	-1.509
N6	-5.483	2.269	-0.233	2.712	-5.676	-0.127	-1.441	0.052	-0.354
N7	-5.367	2.329	-0.074	2.873	-5.475	0.023	-0.343	-0.034	-0.173
N8	-5.417	2.383	-0.019	2.900	-5.477	0.011	-0.020	0.011	-0.038
N9	-5.367	2.328	0.034	2.872	-5.473	0.000	0.295	0.034	-0.190
N10	-5.487	2.270	0.187	2.711	-5.675	0.152	1.395	-0.051	-0.376
N11	-3.525	0.194	0.547	0.024	-3.310	0.285	0.758	0.711	-1.093
N12	-3.058	-0.089	0.281	-0.051	-3.065	-0.337	0.074	0.110	-0.690
N13	-3.063	-0.026	0.053	0.002	-2.977	-0.220	0.026	-0.006	-0.634
N14	-3.062	0.031	-0.072	0.000	-2.978	-0.215	-0.025	-0.011	-0.625
N15	-3.053	0.091	-0.301	0.056	-3.066	-0.329	-0.089	0.103	-0.691
N16	-3.521	-0.195	-0.570	-0.025	-3.310	0.288	-0.792	0.759	-1.166

Table S9. Predicted double-well depths (in unit of eV per formula unit) of LaWN₃, BaTiO₃ and PbTiO₃ based on LDA, PBE and PBEsol functionals. Tetragonal ferroelectric phase (P4mm) is used for BaTiO₃ and PbTiO₃.

	LaWN ₃	BaTiO ₃	PbTiO ₃
LDA	0.109	0.012	0.111
PBE	0.161	0.112	0.555
PBEsol	0.109	0.036	0.196

Table S10. Lengths of La-N bonds (Å) in the surface LaN-layer (Bold); Lengths of La-N bonds in inner LaN-layer are listed in the last three columns (Blue colour). La-N bonds exhibit alternating short and long bond length along the orientation of ferroelectric polarization (*a* direction) due to the ion displacements along this direction. In each LaN-layer, there are four lengths for La-N bonds in the *a-b* plane.

Bonds	1UC	2UC	3UC	4UC	2UC	3UC	4UC
1	2.55	2.49	2.48	2.47	2.62	2.63	2.63
2	2.60	2.61	2.57	2.53	2.73	2.72	2.69
3	2.76	2.88	2.97	3.03	2.73	2.79	2.84
4	2.82	3.01	3.07	3.10	2.88	2.91	2.93

References:

1. J. Padilla and D. Vanderbilt, *Phys. Rev. B*, 1997, **56**, 1625.
2. J. Padilla and D. Vanderbilt, *Surf. Sci.*, 1998, **418**, 64–70.
3. X.-J. Hu, Y. Yang, C. Hou and T.-X. Liang, *J. Phys. Chem. C* 2022, **126**, 517–524.
4. Y. X. Wang, M. Arai, T. Sasaki and C. L. Wang, *Phys. Rev. B*, 2006, **73**, 035411.
5. R. I. Eglitis, *Integr. Ferroelectrics*, 2009, **108**, 11-20.
6. D. Ji, S. Cai, T. R. Paudel, H. Sun, C. Zhang, L. Han, Y. Wei, Y. Zang, M. Gu, Y. Zhang, W. Gao, H. Huyan, W. Guo, D. Wu, Z. Gu, E. Y. Tsymbal, P. Wang, Y. Nie and X. Pan, *Nature*, 2019, **570**, 87-90.
7. A. G. Ricciardulli, S. Yang, J. H. Smet and M. Saliba, *Nature Mater.*, 2021, DOI: 10.1038/s41563-021-01029-9.
8. L. Han, G. Dong, M. Liu and Y. Nie, *Adv. Funct. Mater.*, 2024, **34**, 2309543.
9. Y. Yang, Y.-J. Chen, C. Hou and T.-X. Liang, *J. Phys. Chem. C*, 2022, **126**, 21155-21161.
10. S. Matsuishi, D. Iwasaki and H. Hosono, *J. Solid State Chem.*, 2022, **315**, 123508.
11. K. R. Talley, C. L. Perkins, D. R. Diercks, G. L. Brennecka and A. Zakutayev, *Science*, 2021, **374**, 1488-1491.
12. R. Sarmiento-Perez, T. F. Cerqueira, S. Körbel, S. Botti and M. A. Marques, *Chem. Mater.*, 2015, **27**, 5957-5963.
13. Y.-W. Fang, C. A. J. Fisher, A. Kuwabara, X.-W. Shen, T. Ogawa, H. Moriwake, R. Huang and C.-G. Duan, *Phys. Rev. B*, 2017, **95**, 014111.